RSC Advances

PAPER

View Article Online
View Journal | View Issue

Cite this: *RSC Adv.*, 2025, **15**, 41514

Valorization of coconut water-derived bacterial cellulose in water treatment: environmentally benign modification to enhance the adsorption capacity for multiple heavy metal ions

Ha V. Le,[ab] Dat D. B. Nguyen,[ab] Phu V. Luu,[ab] Uyen T. N. Vy,[ab] Anh T. H. Phan,[ab] Linh H. T. Nguyen,[bc] Phuoc H. Ho,[d] Hanh H. M. Nguyen[ab] and Khoa D. Nguyen *[ab]

Bacterial cellulose, produced through the fermentation of sugar-rich natural resources, exhibits a unique three-dimensional structure and higher purity than plant-derived cellulose, making it promising for various applications. In this study, we modified bacterial cellulose from coconut water using readily available reagents, such as diammonium hydrogen phosphate and urea, without toxic solvents. Characterization techniques, including XPS, SEM-EDX, XRD, FTIR, TGA, and elemental analysis, confirmed successful phosphorylation with a phosphorus substitution degree of up to 11%. We investigated the effects of phosphorylation and adsorption conditions on the uptake of four metal ions (Cu^{2+}, Cd^{2+}, Fe^{3+}, and Pb^{2+}), finding a correlation with phosphorylation efficiency. The adsorption data conformed to the Langmuir model, indicating monolayer adsorption, and kinetic studies suggested that chemisorption should be the dominant mechanism. The study expanded to five additional metal cations, including Ni^{2+}, Cr^{3+}, Zn^{2+}, Co^{2+}, and Mn^{2+}, demonstrating enhanced adsorption capacity due to the phosphorylation. The single-metal uptake ranged from 77.5 to 113.9 mg g^{-1}, exhibiting a 2.3–4.4-fold improvement over unmodified bacterial cellulose. Similar results were obtained for simulated wastewater samples containing all these metal ions. Importantly, the bacterial cellulose-based adsorbent was successfully recovered and reused for four cycles, maintaining considerable capacities. These findings highlight bacterial cellulose as a sustainable, high-quality alternative for water treatment and demonstrate its potential as a value-added functional material derived from sugar-based biomass.

Received 6th August 2025
Accepted 21st October 2025

DOI: 10.1039/d5ra05752c

rsc.li/rsc-advances

Introduction

Water contaminants are increasingly threatening ecosystems due to unsustainable anthropogenic activities. In addition to the widespread presence of organic pollutants such as dyes and oils, heavy metal ions have emerged as particularly hazardous inorganic contaminants that significantly impact aquatic environments.[1] In most cases of water pollution, these toxic metallic components are introduced into natural systems through various industrial activities, including wastewater discharge, mining, metallurgy, leather tanning, electroplating, electrolysis, battery production, textile manufacturing, petroleum refining, paper and pulp processing, and fluidized bed bioreactors.[2,3] It is globally estimated that approximately 380 trillion liters of wastewater are discharged annually, with heavy metals being among the most problematic pollutants.[4] Specifically, in Vietnam, about 30% of the 3 million cubic meters of daily wastewater remains untreated.[5] During their release, heavy metal ions can interact with organic compounds, forming more complex and toxic derivatives, which directly or indirectly infiltrate living systems through various mechanisms such as diffusion and adsorption.[6] The concentration of these ions is critical, as their accumulation, even at trace levels, can lead to severe toxicity. Typical metal ions of Mn, Cu, Co, Fe, Ni, Zn, and Cr can cause serious health issues, including organ damage, cancer, neurological disorders, chronic poisoning, and brain dysfunction.[1,7] These risks underscore the urgent need for effective heavy metal removal techniques to reduce environmental pressure on wastewater resources.

Various approaches have been developed for heavy metal remediation, such as chemical precipitation, chelating

[a]*Faculty of Chemical Engineering, Ho Chi Minh City University of Technology (HCMUT), 268 Ly Thuong Kiet Street, Dien Hong Ward, Ho Chi Minh City, Vietnam. E-mail: khoand1989@hcmut.edu.vn*

[b]*Vietnam National University Ho Chi Minh City, Linh Xuan Ward, Ho Chi Minh City, Vietnam*

[c]*University of Health Sciences (UHS), Vo Truong Toan Street, Dong Hoa Ward, Ho Chi Minh City, Vietnam*

[d]*Chemical Engineering, Competence Centre for Catalysis, Chalmers University of Technology, Gothenburg, SE-412 96, Sweden*

precipitation, coagulation and flocculation, flotation, electrochemical treatment, photocatalysis, ion exchange, membrane filtration, biological treatment, and adsorption.[8–12] However, many of these techniques face undeniable disadvantages. For instance, chemical methods often generate large volumes of sludge as secondary waste, while membrane filtration suffers from high installation costs and periodic fouling.[2,13] Among these, adsorption is widely regarded as the most cost-effective and efficient method, wherein heavy metal ions are captured on the surface or within the porous structure of adsorbents, with potential for regeneration and reuse.[14,15] Although traditional adsorbents such as activated carbon, alumina, zeolites, clays, and carbon nanotubes are widely used, there is growing interest in green alternatives derived from biomass and agricultural waste, valued for their renewability, low cost, and environmental friendliness.[1,16,17] Notably, cellulose, abundant in nature, along with hemicellulose, lignin, and pectin, has attracted attention as a promising adsorbent for heavy metals remediation in water through efficient and diverse surface functionalizations or adjustable combinations with other materials.[18–21] Nevertheless, plant-based cellulose typically requires extensive pretreatment involving harsh alkaline chemicals and bleaching agents, which are energy-intensive, time-consuming, and environmentally detrimental.[22,23] In contrast, bacterial cellulose (BC), synthesized *via* microbial fermentation of sugar-based media under mild conditions, offers a more sustainable alternative.[24,25] BC consists of an interconnected nanofibrous network with distinct advantages, including high crystallinity (>84%), high purity (free from other biopolymers), excellent water-holding capacity, and superior mechanical properties.[26] Interestingly, our recent study has shown that pristine BC could adsorb a variety of metal ions, albeit with relatively low capacities (6.0–45.0 mg g^{-1}).[26] Therefore, chemical modifications are typically necessary for the cellulose matrix to adjust the surface properties and improve the adsorption of the metal ions.[1,27] The general strategy for this modification involves grafting functional groups *via* typical organic reactions with the abundant hydroxyl sites of cellulose, such as esterification, etherification, phosphorylation, halogenation, oxidation, or silylation. Among them, the phosphorylation route has been widely applied due to its simplicity and high efficiency.[28,29] Namely, the hydroxyl groups on the cellulose backbone can be converted into phosphate [–O–P(=O)$(OH)_2$], phosphite [–O–P$(OH)_2$], or phosphonic acid [–P(=O)$(OH)_2$] groups, which are expected to result in increasing the surface negative charge, thereby attracting more positively charged metal ions.[23,30–33] As can be expected, phosphorylated cellulose was demonstrated to possess a large number of phosphate-based acidic sites, which can be used as scaffolds for ion exchange.[34] To perform the phosphorylation of cellulose, phosphoryl chloride ($POCl_3$) could be used, affording good removals of Cd^{2+}, Cr^{3+}, and Pb^{2+}.[23] However, the high toxicity and high cost of $POCl_3$ and corrosive by-products, *e.g.*, HCl, limited its practical application. On the other hand, Oshima *et al.* synthesized phosphorylated bacterial cellulose to adsorb a variety of lanthanide and transition metal ions, and proteins. The pathway reported in this study for modifying bacterial cellulose showed a high degree of phosphorylation (up to 21.8%) but required phosphoric acid as a phosphate source in the presence of *N*,*N*-dimethylformamide as the solvent.[30,31] In addition, the poor adsorption performance (<5 mg g^{-1}) of the obtained material was recorded for common metal ions. Alternatively, less hazardous phosphate salts such as $NH_4H_2PO_4$, NaH_2PO_4, Na_2HPO_4, and LiH_2PO_4 have been successfully employed in combination with molten urea for the phosphorylation of cellulose, which was almost extracted from various plant-based sources *via* harsh alkaline treatments.[23,30,35,36] Meanwhile, the interaction between phosphate salts, urea, and bacterial cellulose under environmentally benign conditions towards developing an efficient adsorbent for heavy metal removal remains underexplored. Therefore, in this study, we aimed to systematically investigate the adsorption behaviour of phosphorylated bacterial cellulose for a variety of metal ions, focusing on crucial parameters related to both phosphorylation of BC and adsorption of metal ions. This work is expected to further valorise bacterial cellulose as an abundant biomass resource for the development of green, high-performance materials for water treatment.

Experimental

Materials

Chemicals including diammonium hydrogen phosphate ($(NH_4)_2HPO_4$), urea ($(NH_2)_2CO$), sodium hydroxide (NaOH), hydrochloric acid (HCl), aluminum nitrate nonahydrate ($Al(NO_3)_3 \cdot 9H_2O$), chromium(III) nitrate nonahydrate ($Cr(NO_3)_3 \cdot 9H_2O$), manganese(II) acetate tetrahydrate ($(CH_3COO)_2Mn \cdot 4H_2O$), iron(III) nitrate nonahydrate ($Fe(NO_3)_3 \cdot 9H_2O$), cobalt(II) nitrate hexahydrate ($Co(NO_3)_2 \cdot 6H_2O$), nickel(II) nitrate hexahydrate ($Ni(NO_3)_2 \cdot 6H_2O$), copper(II) acetate monohydrate ($Cu(CH_3COO)_2 \cdot H_2O$), zinc nitrate tetrahydrate ($Zn(NO_3)_2 \cdot 4H_2O$), cadmium(II) acetate ($Cd(CH_3COO)_2$), and lead(II) nitrate ($Pb(NO_3)_2$) were purchased from Sigma-Adrich and Fisher Scientific.

Synthesis of phosphorylated bacterial cellulose

Bacterial cellulose (BC) was synthesized in the form of hydrogel sheets (BC content = approximately 0.8%) through the fermentation of coconut water using *Acetobacter xylinum*, following a previously reported method.[24,37,38] The raw BC sheets were immersed in a 1 M NaOH solution for 12 h, then washed with water until reaching a neutral pH. Afterward, the sheets were cut into 1-cm cubes (Fig. 1a). A mixture of these BC pieces (125 g) and water (125 g) was homogenized using a Philips HP1600 hand blender (550 W) for 2 min, yielding a uniform BC suspension (Fig. 1b).

For the phosphorylation process, a typical experiment involved mixing 250 g of the prepared BC suspension (containing 1 g of BC) with $(NH_4)_2HPO_4$ (5.1 g) and $(NH_2)_2CO$ (9.0 g) under vigorous stirring for 1 h. The mixture was distributed into 50-mL porcelain crucibles. In an oven, partial dehydration was performed at 60 °C for 12 h, followed by the thermal phosphorylation stage at 150 °C for 1 h. After cooling, the samples were thoroughly washed with excess deionized water to remove

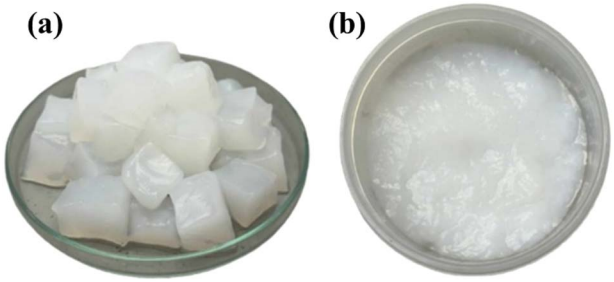

Fig. 1 Photographs of (a) BC hydrogel pieces, (b) suspension of well-ground BC in water.

unreacted chemicals, yielding water-saturated hydrogels of phosphorylated BC which was denoted as PBC *X*/*Y*/*Z* (Table 1) in which *X*, *Y*, and *Z*, respectively, was the phosphorylation temperature (120–160 °C), the phosphorylation time (0.0–2.0 h), and the urea amount used (0–12 g).

Characterization of the materials

Scanning electron microscopy (SEM) for the pristine and phosphorylated bacterial cellulose samples was performed using a TM4000 microscope (Hitachi, Japan) at 15.0 kV with varying magnifications. SEM analysis was complemented by energy-dispersive X-ray spectroscopy (EDX), including elemental mapping. X-ray photoelectron spectroscopy (XPS) was conducted on an ESCALAB 250 spectrometer (VG Scientific, UK) equipped with an Al Kα radiation source (1486.6 eV). Powder X-ray diffraction (XRD) patterns were collected on a D8 Advance diffractometer (Bruker, Germany) using Cu Kα radiation in a 2θ range of 10–70° with 0.01° per step and a scanning rate of 0.6° min^{-1}. Fourier transform infrared spectra (FTIR) were obtained using an Alpha II spectrometer (Bruker, Germany) in the wavelength range of 4000–500 cm^{-1}, with a resolution of 2 cm^{-1} over 32 scans. Thermogravimetric analysis (TGA) was conducted using a TGA/DSC 3+ system (Mettler Toledo, Switzerland) in the temperature range of 25–800 °C at a rate of 10 °C min^{-1} under an air flow.

The degree of phosphorous substitution (DPS) was determined using eqn (1).[39,40]

$$\frac{162.1\%\ P}{3100 - 64\%\ P} \quad (1)$$

where %*P* was the total phosphorus content determined by ultraviolet-visible (UV-Vis) spectroscopy. In detail, the bacterial cellulose-based sample was digested into a solution containing inorganic phosphate, if any, which was followed by complexing with ammonium molybdate(VI) for the UV-Vis analysis at 690 nm using a GENESYS 50 spectrophotometer (Thermo Scientific, United States).

The point of zero charge (PZC) of the materials was determined by a salt addition method. Prior to the measurement, a 0.1 M NaCl solution was prepared, and its initial pH (pH_i) was adjusted using diluted HCl or NaOH solutions. The sample was then introduced into the solution and stirred at room temperature. After equilibrium, the final pH (pH_f) was recorded. The difference ($\Delta pH = pH_f - pH_i$) was plotted as a function of pH_i, and the PZC value was recorded as the intersection point where $\Delta pH = 0$.[41]

Adsorption experiment for heavy metal ions

In a typical adsorption experiment for a single metal ion, 5.00 g of the hydrogel-form cellulose material containing 0.04 g of modified bacterial cellulose was added to a 20-mL vial containing 10 mL of an aqueous metal ion solution, which was prepared by dissolving the corresponding metal salt in water. The adsorption process was carried out under vigorous stirring at room temperature for a predetermined duration.

After the adsorption course, the liquid was collected *via* simple filtration and subsequently analysed with atomic absorption spectrometry (AAS) to determine the residual metal ion concentration, using a DW-AA4530F spectrophotometer (Drawell, China).

Table 1 Details on the synthesis conditions for the phosphorylated BC samples

Entry	Sample	Phosphorylation temperature (°C)	Phosphorylation time (h)	Urea amount (g)	Degree of phosphorylation (%)
1	Pure BC	0	0.0	0	—
2	PBC 120/1.0/12	120	1.0	12	6.60
3	PBC 130/1.0/12	130	1.0	12	6.47
4	PBC 140/1.0/12	140	1.0	12	7.71
5	PBC 150/1.0/12	150	1.0	12	10.99
6	PBC 160/1.0/12	160	1.0	12	8.69
7	PBC 12	—	—	12	1.39
8	PBC 150/0.5/12	150	0.5	12	4.96
9	PBC 150/1.5/12	150	1.5	12	7.79
10	PBC 150/2.0/12	150	2.0	12	5.89
11	PBC 150/1.0/0	150	1.0	0	5.92
12	PBC 150/1.0/3	150	1.0	3	6.44
13	PBC 150/1.0/6	150	1.0	6	7.94
14	PBC 150/1.0/9	150	1.0	9	7.88

The adsorption capacity was calculated based on the difference in metal ion concentrations before and after adsorption, as expressed by eqn (2).

$$q_m = \frac{(C_0 - C)V_m}{m} \quad (2)$$

where q_m (mg g^{-1}) is the adsorption capacity of the material for the corresponding metal ion, C_0 (ppm) is its initial concentration, C (ppm) is its concentration after the adsorption course, V_m (L) is the total solution volume, and m (g) is the cellulose mass of the material.

The obtained adsorption data at various contact times were used to determine the kinetic adsorption models, namely pseudo-first-order and pseudo-second-order, as introduced in previous work.[26,33] These two models were described as eqn (3) and (4).

$$\ln(q_e - q_t) = \ln q_e - k_1 t \quad (3)$$

$$\frac{t}{q_t} = \frac{1}{k_2 q_e^2} + \frac{1}{q_e} t \quad (4)$$

where q_e (mg g^{-1}) and q_t (mg g^{-1}) are the adsorption capacity for the metal ions at the equilibrium state and at a given time (t, min), k_1 (1 min^{-1}) and k_2 (g mg^{-1} min^{-1}) are the rate constants of the models, respectively.

In addition, two typical Langmuir and Freundlich isotherm models, as expressed by eqn (5) and (6), were explored based on the initial metal concentration-dependent adsorption results.[42]

$$\frac{1}{q_e} = \frac{1}{q_{max} K_L C_e} + \frac{1}{q_{max}} \quad (5)$$

$$q_e = K_F C_e^{\frac{1}{n}} \quad (6)$$

where q_e (mg g^{-1}) is the adsorption capacity for the metal ion at the equilibrium state, q_{max} (mg g^{-1}) is the metal ion adsorption capacity, C_e is the equilibrium concentration in the metal ion solution, K_L (L mg^{-1}) and K_F [(mg g^{-1})(L g^{-1})$^{1/n}$ are the Langmuir and Freundlich adsorption isotherm constants, respectively, n is the dimensionless constant related to the adsorption intensity.

To investigate the adsorption performance of PBC for multi-metal ions, 5 g of the hydrogel-form cellulose material containing 0.04 g of modified bacterial cellulose was added to 10 mL of an aqueous solution containing 9 metal ions, namely, Cr^{3+}, Ni^{2+}, Fe^{3+}, Mn^{2+}, Co^{2+}, Cu^{2+}, Zn^{2+}, Cd^{2+}, and Pb^{2+}, with a concentration of 50 ppm for each. The concentration of each metal in the solution after the adsorption course was determined by inductively coupled plasma-optical emission spectrometry (ICP-OES) using an Optima 7000 DV device (PerkinElmer, United States).

Recycling test

After the adsorption experiment for the single metal ion, spent phosphorylated bacterial cellulose was dispersed in 10 mL of a 10% NH_4Cl solution for 5 h to desorb the metal species. Such ion exchange was repeated three times, followed by washing with water until neutralization. The obtained bacterial cellulose phase was reused for the adsorption cycle under the identical conditions.

Results and discussion

Characterization of phosphorylated bacterial cellulose

Pristine BC exhibited a naturally white appearance due to its high cellulose purity while the as-prepared PBC samples displayed a colour transition to yellow or orange depending on the treatment temperature (Fig. 2a–d). Notably, at a phosphorylation temperature of 160 °C, brown spots appeared on the PBC surface (Fig. 2e), suggesting partial carbonization of the cellulose under elevated thermal conditions.[43,44] These impurities were effectively removed during the water-washing process, resulting in yellow, hydrogel-form PBC samples for further characterization (Fig. 2f–j). Morphological changes of the BC material, if any, upon phosphorylation were discovered using SEM (Fig. 3). In its native form, BC exhibited a distinct three-dimensional (3D) fibrous network, indicative of strong intermolecular interactions among cellulosic units (Fig. 3a and b). After the phosphorylation, particularly at 150 °C, for 1 h, the fibrous network appeared partially disrupted, with some cellulose fibers detached from the matrix (Fig. 3c and d), confirming the structural transformation due to phosphorylation. Elemental mapping further validated the successful incorporation of phosphorus groups, showing a homogeneous

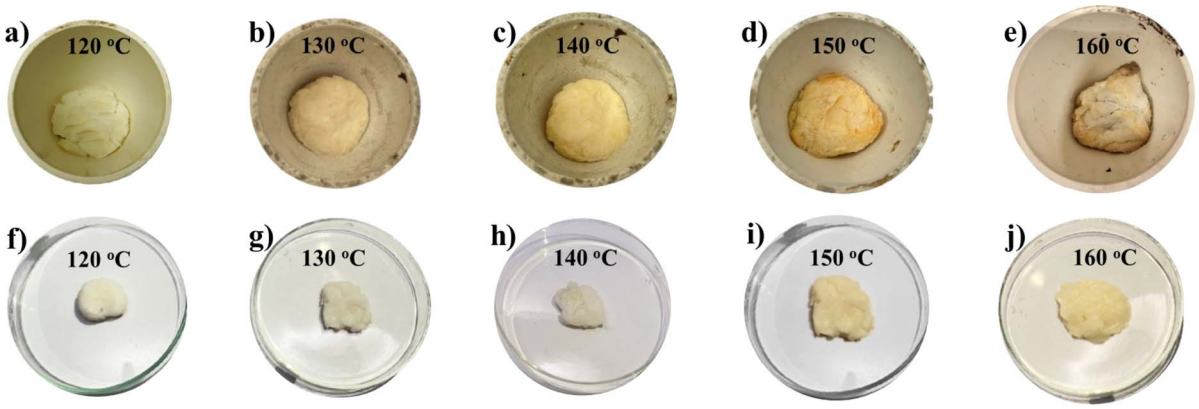

Fig. 2 (a–e) PBC samples after the thermal treatment at the specific temperatures, (f–j) corresponding PBC samples after washing with water.

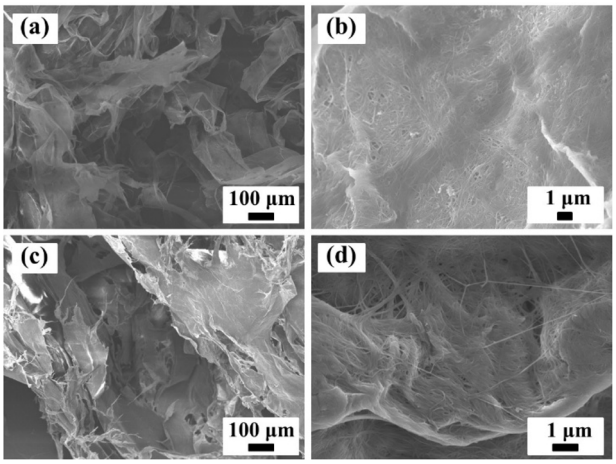

Fig. 3 SEM images of (a and b) pristine BC and (c and d) PBC 150/1.0/12.

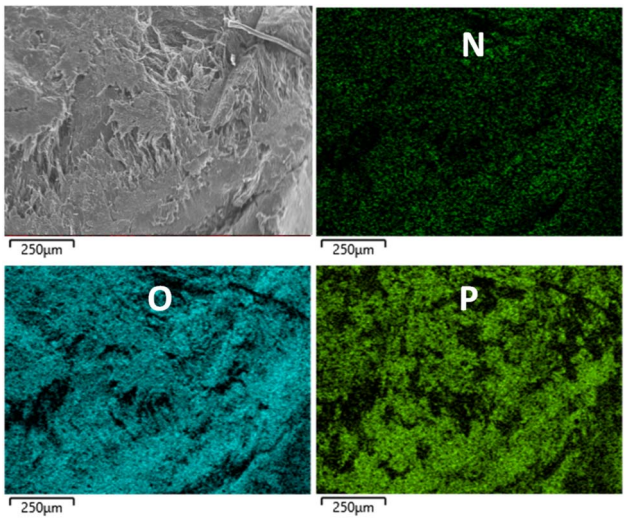

Fig. 4 Selected SEM area and corresponding EDX mapping of oxygen, nitrogen, and phosphorus for PBC 150/1.0/12.

distribution of oxygen and phosphorus across the PBC surface (Fig. 4a–d). Although nitrogen was also detected, its signal was less defined, suggesting a high degree of phosphorylation alongside a limited retention of urea-derived nitrogen species.

The XRD patterns of pristine and phosphorylated bacterial cellulose materials are presented in Fig. 5. The diffraction pattern of pure BC displayed three distinct peaks at $2\theta = 14.8$, 16.7, and 22.5°, corresponding to the $(\bar{1}10)$, (110), and (200) planes of cellulose *I* (JCPDS #03-0829), which usually involves both I_α and I_β allomorphs. This result aligned with previous findings that identified cellulose *I* as the dominant crystalline phase in bacterial cellulose.[45–47] Importantly, the PBC samples also showed these characteristic peaks, indicating that a similar crystallinity of the cellulose network was retained after the phosphorylation. However, an additional diffraction peak emerged at $2\theta = 29.7$ and 34.7°, corresponding to the $(\bar{1}22)$ and (004) planes, which are sometimes observed for the cellulose-

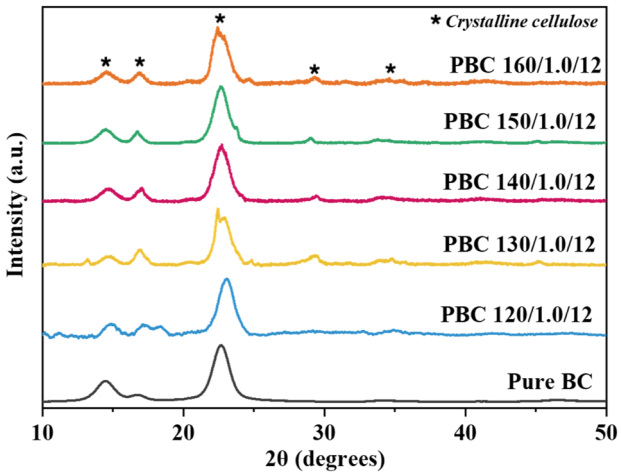

Fig. 5 XRD patterns of pure BC and PBC.

based phases. The appearance of this new peak suggests a partial rearrangement of the cellulose crystalline framework induced by phosphorylation treatment.[45,48,49] Moreover, compared to pristine BC, the XRD profiles of the PBC samples exhibited broader and less defined peaks, indicating a reduction in crystallinity and structural disorder resulting from chemical modification. These observations are consistent with prior studies that reported similar changes in cellulose crystallinity upon chemical treatment, such as alkali modification with NaOH under thermal conditions.[49,50] The altered diffraction patterns further confirm the structural transformation of BC during the phosphorylation.

FTIR spectra of phosphorylated bacterial cellulose (PBC) synthesized at various temperatures (120 to 160 °C), along with that of native bacterial cellulose (BC), are presented in Fig. 6. The spectrum of pristine BC exhibited a broad absorption band between 3342–3230 cm^{-1}, corresponding to the stretching

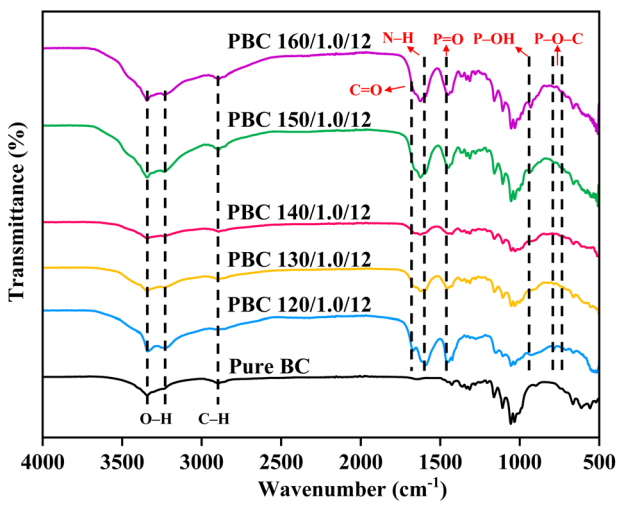

Fig. 6 FTIR spectra of pure BC and PBC.

vibrations of both inter- and intramolecular O–H bonds.[51] A peak at 2894 cm^{-1} was also observed, attributed to the asymmetric stretching of Csp^3–H bonds.[52,53] These characteristic features are consistent with the well-established molecular structure of bacterial cellulose, which is rich in hydroxyl groups and frequently reported in the literature.[53,54] In the fingerprint region (1500–500 cm^{-1}), other peaks of cellulose were evident, including bands at 1427, 1368, 1337, and 1315 cm^{-1} corresponding to the bending and stretching vibrations of $-CH_2$, –CH, –OH, and C–O bonds.[55] The peaks in the 1165–1120 cm^{-1} range were assigned to asymmetric stretching of the C–O–C bond in β-(1,4)-glycosidic linkages, while the peak at 1033 cm^{-1} was associated with skeletal vibrations of the pyranose ring.[56,57]

The phosphorylation of BC could be confirmed by the emergence of additional bands in the FTIR spectra of PBC, attributed to phosphate-related functional groups such as O–P–OH, P═O, P–OH, and P–O–C.[58] A new band at 1455 cm^{-1}, which became sharper with increasing temperature, was assigned to the P═O vibration of orthophosphate diesters.[59] Furthermore, a prominent P–OH stretching band at 931 cm^{-1} was observed in the samples treated at higher temperatures, namely, 150 and 160 °C. The formation of P–O–C aliphatic linkages was evidenced by bands appearing in the 831–785 cm^{-1} range at temperatures above 130 °C.[60] These results underscore the critical role of temperature in facilitating phosphorylation. Zhang *et al.* reported that urea began to decompose at about 130 °C and effective phosphorylation occurred only above 150 °C.[61] Additionally, the bands at 1670 and 1590 cm^{-1} were attributed to the vibration of the C═O and N–H groups, while they were not found for the urea-free sample (Fig. S2). These spectral results proved the successful incorporation of urea into the material under the phosphorylation conditions.[62] Importantly, the FTIR spectra of the PBC samples after metal ion adsorption revealed the complete disappearance of the P–OH stretching band at 931 cm^{-1}. This spectral change strongly suggested that the P–OH functional groups were involved in the adsorption process through chemical interactions with the metal ions. The loss of this vibrational signal was indicative of a possible coordination or complexation mechanism, whereby the P–OH groups can donate lone pairs of electrons to the metal cations, forming stable P–O–metal linkages. Therefore, it can be conclusively inferred that the P–OH moieties introduced during phosphorylation should be the major active sites for metal ion binding in PBC. The functional role of P–OH groups in mediating the interaction with metal ions further underscored the effectiveness of phosphorylation in enhancing the metal-binding performance of bacterial cellulose.[63,64]

TGA was conducted in air to elucidate the temperature-dependent decomposition behaviour of unmodified and phosphorylated bacterial cellulose samples (Fig. 7). Two distinct mass-loss stages were generally identified, including moisture removal and thermal degradation. During the physical dehydration (100–200 °C), both free and adsorbed water molecules were released. Pristine bacterial cellulose showed a relatively low moisture loss, with a weight reduction of approximately 7.2 wt% at 200 °C. In contrast, the phosphorylated bacterial cellulose sample exhibited significantly higher weight losses, up

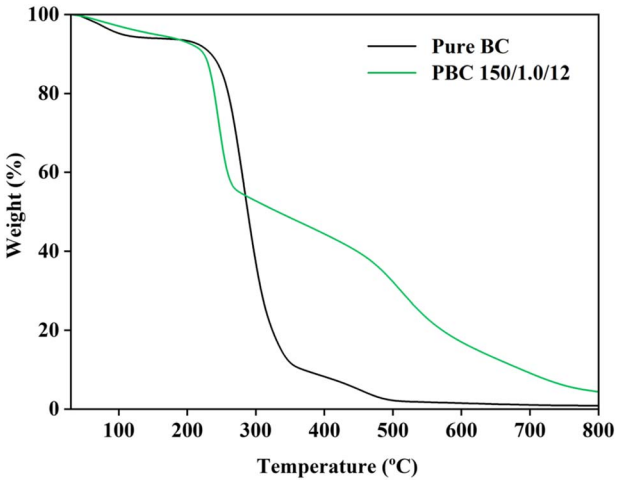

Fig. 7 TGA profiles of pure BC and PBC 150/1.0/12.

to 20 wt% under the same conditions. Such a high moisture uptake in PBC could be attributed to the substitution of hydroxyl groups with phosphate moieties, which might increase hydrophilicity and thereby water-binding capacity of the resulting material.

In the temperature range of 200 to 400 °C, commonly associated with the thermal degradation of cellulose, a major mass loss was observed in unmodified BC. The sample weight decreased fast to approximately 10 wt% at 350 °C and continued to decline, leaving only a small residue amount (0.84 wt%) at 800 °C. This weight loss reflected the decomposition of the cellulose polymer through chemical dehydration, pyrolysis, oxidation and combustion in the presence of oxygen, leading to the emission of gaseous products, *e.g.* CO and CO_2.[65,66] Notably, the decomposition of the PBC sample underwent two clear steps from 200 to 800 °C. The first degradation stage in a short temperature range (200–250 °C) caused the PBC weight to increase by about 33 wt%, resulting from the dehydration of the cellulose-based hydroxyl groups.[67] The carbon- and phosphorus-enriched phase served as a protective barrier, slowing down the overall degradation rate and yielding a non-volatile residue of ~5 wt% at 800 °C.[34,61] This residual char might involve thermally stable aromatic and phosphate-based structures that resisted volatilization under such a harsh condition. Furthermore, the enhanced thermal stability of PBC highlights the significant influence of chemical modification on cellulose pyrolysis pathways, suggesting that the phosphoryl functionalization can tailor the thermal response of cellulose-based composites for specific applications.

The XPS result of PBC 150/1.0/12 (Fig. S1) identified its surface elemental composition and the oxidation state of the present elements. Indeed, the C 1s peak might include three member peaks assigned to the C═O/O–C–O (288.3 eV), –CH–O (286.4 eV), and $-CH_2O$ (284.9 eV) groups (Fig. 8a), representing the typical bonds of carbon in the cellulose chain as presented in the literature.[68–70] Similarly, the O 1s spectrum (Fig. 8b) displayed a high-intensity peak at 533.7 eV related to the oxygen atoms in the hydroxyl and glycoside groups of cellulose.

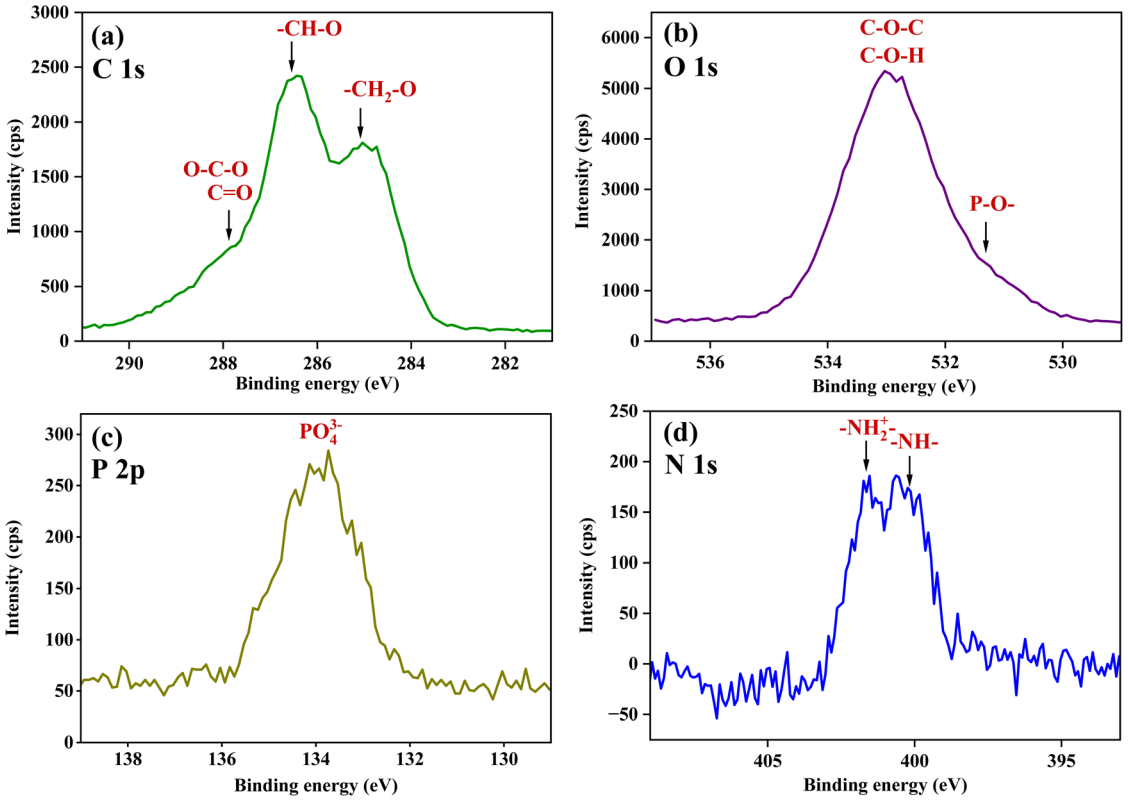

Fig. 8 XPS spectra of (a) C 1s, (b) N 1s, (c) O 1s and (d) P 2p for PBC 150/1.0/12.

Notably, a shoulder peak appeared at approx. 531 eV, which could be attributed to the O species of the grafted phosphate group.[44,71] In addition, the successful functionalization of BC with the phosphate species could be confirmed by the presence of the P 2p peak at 134 eV, which has been considered as a characteristic peak of P(V) in the phosphate group (Fig. 8b).[43,60,72] The spectrum of N 1s showed two main peaks around 400 and 402 eV, which can be attributed to protonated amine (–NH_2^+–) and amine (–NH–) groups. This observation was consistent with the earlier reports showing a minor shift in the nitrogen binding energy due to the protonation, *e.g.*, for polypyrrole particles and other nitrogen-containing compounds like pyridine dicarboxylic acid and polyaniline.[73–76] The amine-based nitrogen atoms in the PBC, derived from urea and the ammonium salt for the phosphorylation process, could serve as the cationic partner for the phosphate groups (Fig. 9).[28,76,77] It was previously proposed that urea could be thermally decomposed into isocyanic acid, which further reacted with cellulose to form cellulose carbamate; therefore, its presence in PBC as a side functionality should not be ruled out.[78,79]

Adsorption studies

Due to the thermal modification, the phosphorylation temperature plays a critical role in regulating the modification of functional groups on the surface of bacterial cellulose. The impact of phosphorylation temperature on the adsorption performance of phosphorylated bacterial cellulose (PBC) was discovered and presented in Fig. 10. Even under the mildest treatment condition of 120 °C, the PBC sample (PBC 120/1.0/12) exhibited significantly improved adsorption capacities compared to pristine BC, with the uptake values ranging from 38.26 to 46.28 mg g^{-1} for the tested metal ions.[80] Further increasing the phosphorylation temperature from 140 to 150 °C resulted in significant enhancements in the adsorption of Cu^{2+} and Pb^{2+}, while the adsorption of Fe^{3+} and Cd^{2+} exhibited less increase in this case. It was elucidated that above the melting point of urea (130 °C), urea acted as a molten solvent, facilitating better penetration and interaction of the phosphate reagent with the cellulose matrix and supporting the structural preservation of the BC network.[29] Importantly, increasing the temperature from 120 to 150 °C accelerated the phosphorylation efficiency, which was confirmed by a noticeable growth in the degree of phosphorus substitution from 6.60 to 10.99% (entries 2–5, Table 1). This functionalization enhancement directly correlated with the improved adsorption performance of PBC in forwarding metal ions.

However, a clear decrease in the adsorption capacity for all four metal ions was observed for the sample prepared at 160 °C, suggesting that excessive thermal treatment may adversely affect the structural integrity or surface functionality of the material. Within this study scope, 150 °C was recorded as the optimal phosphorylation temperature, yielding the highest adsorption capacities ranging from 45.09 to 51.61 mg g^{-1} for all studied metal ions. Although higher temperatures likely enhanced phosphate group grafting, the structural degradation

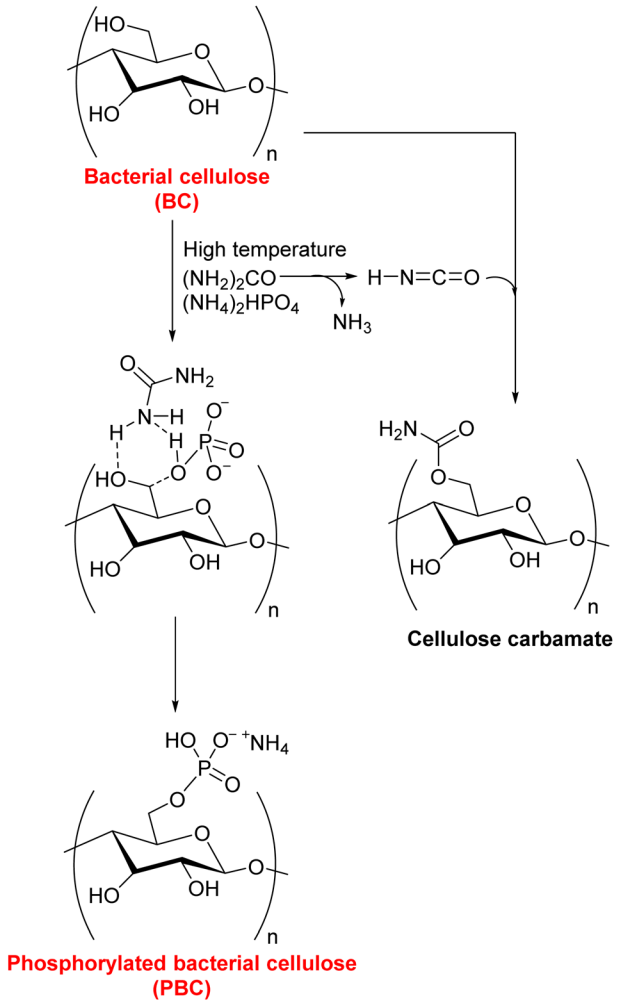

Fig. 9 Proposed phosphorylation mechanism.

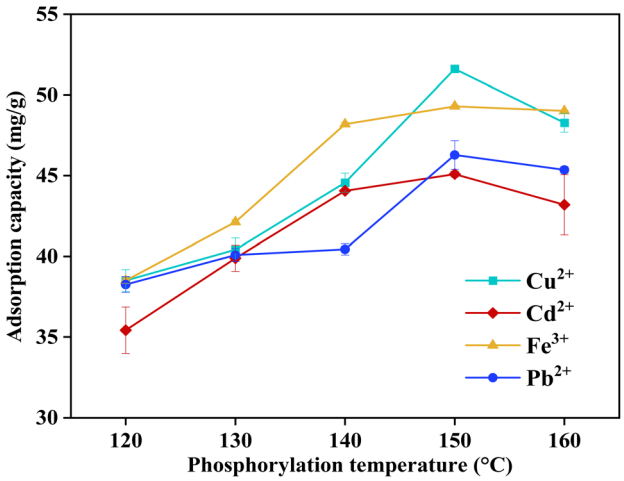

Fig. 10 Effect of the phosphorylation temperature on the adsorption capacity of PBC (phosphorylation conditions: time 1 h, urea 12 g; adsorption conditions: dosage 0.04 g/10 mL, concentration 200 ppm, temperature 30 °C, time 120 min, pH 5.0 ± 0.2, for Fe^{3+} pH 2.5).

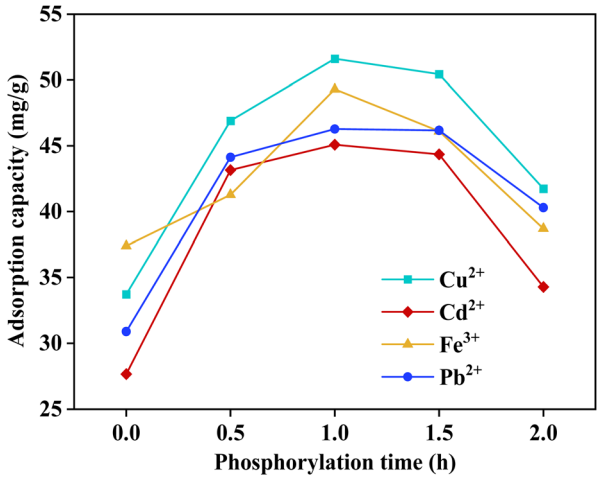

Fig. 11 Effect of the phosphorylation time on the adsorption capacity of PBC (phosphorylation conditions: temperature 150 °C, urea 12 g; adsorption conditions: dosage 0.04 g/10 mL, concentration 200 ppm, temperature 30 °C, time 120 min, pH 5.0 ± 0.2, for Fe^{3+} pH 2.5).

of the cellulose network might occur under harsh conditions in the presence of the acidic reagents. As expected, the degree of phosphorus substitution at 160 °C decreased to 8.69%. According to the obtained results, a phosphorylation temperature of 150 °C was proposed for subsequent studies, generally aligning well with the 150–165 °C range reported in previous studies utilizing molten urea and diammonium phosphate as phosphorylation agents for cellulose.[29,81]

The effect of the phosphorylation time on the adsorption performance of phosphorylated bacterial cellulose was investigated, as shown in Fig. 11. The control sample (PBC 12), which lacked the thermal treatment at 150 °C, exhibited the lowest adsorption capacities of 27.65, 30.89, 33.72, and 37.40 mg g^{-1} for Cd^{2+}, Pb^{2+}, Cu^{2+}, and Fe^{3+}, respectively, confirming the necessity of thermal activation in facilitating the successful incorporation of phosphate groups onto the cellulose surface towards the enhanced metal ions uptake. Upon phosphorylation at 150 °C, the adsorption capacities of all metal ions increased significantly, reaching the highest values after 1 h of thermal treatment. At this optimal reaction duration, Cu^{2+} exhibited the highest adsorption value of 51.61 mg g^{-1}, significantly surpassing the adsorption capacities recorded for Cd^{2+} (45.09 mg g^{-1}), Fe^{3+} (49.30 mg g^{-1}), and Pb^{2+} (46.28 mg g^{-1}). Interestingly, Fe^{3+} showed the highest molar uptake. The superior affinity of PBC for the Fe^{3+} species might be attributed to both the strong chelating ability of phosphate groups and the ionic radius and charge density of Fe^{3+}, which significantly influenced their interaction with the functionalized cellulose matrix. This one-hour phosphorylation period is also commonly adopted in earlier studies to achieve efficient grafting of phosphate groups.[60,82]

On the other hand, extending the phosphorylation time beyond 1 h resulted in a significant decline in the adsorption capacity, which decreased to approximately one-fifth of the maximum value after the two-hour treatment at 150 °C. This

decrease could be attributed to the degradation of the cellulose matrix at an elevated temperature. The phosphorylation process involves the thermal decomposition of $(NH_4)_2HPO_4$, which provides protons necessary for promoting esterification reactions between phosphate ions and hydroxyl groups on the cellulose backbone. While this reaction was favorable in the initial phase, prolonged thermal exposure could lead to excessive proton release, accelerating the dehydration of hydroxyl groups and the hydrolysis of ether bonds within the cellulose chains, resulting in partial depolymerization.[42] Such degradation not only reduced the number of active sites for the phosphate substitution but also weakened the mechanical and chemical stability of the 3D nanofibrous structure of BC. Consequently, in the subsequent washing step, degraded fragments of the cellulose network may leach into water, thereby decreasing the overall yield and functional surface area of the final PBC product. This proposal could be strengthened by the observation that the adsorption performance of the PBC sample prepared at the different phosphorylation times was directly proportional to the degree of phosphorus substitution in these samples. Namely, when the reaction was performed for 1 h, the highest DPS value of 10.99% was obtained. And DPS significantly dropped to 5.89% for the sample phosphorylated for 2 h. It can be concluded that a crucial balance should be required as considering phosphorylation conditions to achieve maximal functionalization while preserving the structural features of bacterial cellulose.

The presence of urea could increase cellulose swelling and protect its structural integrity during phosphorylation by reinforcing the 3D network of bacterial cellulose.[83] This stabilizing effect was therefore essential during the high-temperature treatment as it maintained the cellulose framework, thereby improving the overall phosphorylation yield. Following phosphorylation and washing steps, the BC matrix may reconstruct its original hydrogel form in the presence of water. Therefore, the inclusion of urea is critical in maintaining the cellulose framework, thereby improving the overall phosphorylation yield. The importance of urea was clearly demonstrated by the poor degree of phosphorus substitution and adsorption performance of the PBC 150/1.0/0 sample, which was obtained under the urea-free conditions. This sample exhibited the lowest DPS value of 5.92% (entry 11, Table 1) and thereby the lowest adsorption capacities of 25.58, 22.29, 39.52, and 31.72 mg g^{-1} for Cu^{2+}, Cd^{2+}, Fe^{3+}, and Pb^{2+}, respectively (Fig. 12). As urea with an increasing amount was added to the phosphorylation mixture, significant enhancements in the adsorption capacity for all metal ions were observed, in direct correlation with the degree of phosphorus substitution (entries 12–14, Table 1). However, further increasing the urea content from 9 to 12 g resulted in only minor performance improvements, indicating that 9 g of urea was sufficient to reach an effective molten state for the chemical modification. This urea amount not only supported the preservation of the cellulose network during the thermal treatment but also contributed to a higher number of active phosphate groups, likely due to increased accessibility and reactivity of the cellulose hydroxyls.[83] Although the great DPS improvement of about 40% (from 7.88 to 10.99%, entries 5 and 14, Table 1) was recorded when the urea amount increased from 9 to 12 g, the adsorption performance of PCC for all metal ions increased inconsistently, suggesting that not all phosphorus-based moieties grafted on the cellulose backbone were able to capture the metal ions.

The influence of the contact time on the adsorption of heavy metal ions by phosphate-based cellulose was discovered, and the results are presented in Fig. 13. During the initial 5 min of the adsorption course, a rapid increase in the adsorption capacity was observed for all studied metal ions, affording values of 31.64, 39.25, 45.11, and 35.84 mg g^{-1} for Cu^{2+}, Cd^{2+}, Fe^{3+}, and Pb^{2+}, respectively. This rapid uptake was attributed to the availability and strong affinity of active sites on the PBC surface, which facilitate adsorption driven by an initial high concentration of metal ions.[84] However, as the contact time was

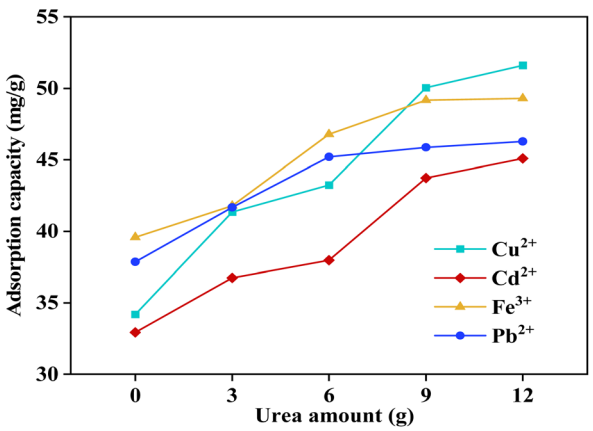

Fig. 12 Effect of the urea amount on the adsorption capacity of PBC (phosphorylation conditions: temperature 150 °C, time 1 h; adsorption conditions: dosage 0.04 g/10 mL, concentration 200 ppm, temperature 30 °C, time 120 min, pH 5.0 ± 0.2, for Fe^{3+} pH 2.5).

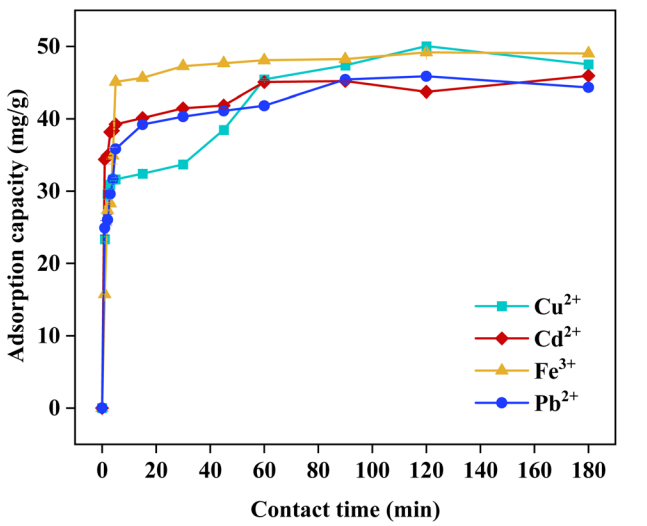

Fig. 13 Effect of the contact time on the adsorption capacity of PBC 150/1.0/9 (adsorption conditions: dosage 0.04 g/10 mL, concentration 200 ppm, temperature 30 °C, pH 5.0 ± 0.2, for Fe^{3+} pH 2.5).

prolonged, the difference in the metal concentration in the PBC network and the solution was less significant. As a result, the driving force for metal ion adsorption gradually decreases, decelerating the adsorption process. Indeed, the adsorption capacity for Fe^{3+} remained almost unchanged after 5 min, while the Cd^{2+} and Pb^{2+} uptakes increased at relatively slow rates. However, Cu^{2+} adsorption required a much longer contact time, namely 120 min, to reach saturation at about 50 mg g^{-1}. As mentioned above, the distinct adsorption performance of Fe^{3+} compared to that of the divalent ions could be explained based on its trivalence and small ionic radius. The combination of a higher charge density and a smaller size enhances electrostatic attraction to the phosphate functional groups on the PBC surface, resulting in more efficient, rapid adsorption. This explanation also aligns with the previously reported study, in which the adsorption of heavy metals by porous NaA zeolite/carbon composites was investigated, and Fe^{3+} demonstrated a superior adsorption performance than Ni^{2+}.[85]

To investigate the mechanism of metal ions adsorption by cellulose-based materials, two kinetic models of adsorption, including pseudo-first-order and pseudo-second-order models (Fig. 14a and b) were applied. As shown in Table S1, the calculated equilibrium adsorption capacities ($q_{e,cal}$) of the pseudo-second-order model for the metal ions fitted better to the experimental values ($q_{e,exp}$). Higher determination coefficients ($R^2 \geq 0.999$) were obtained for the former model compared to those derived from the pseudo-first-order model ($R^2 \leq 0.780$), suggesting that the metal ions adsorption occurred in the pseudo-second-order kinetic model, in which chemisorption should be the dominant mechanism, in good agreement with our previous study on the unmodified BC material.[26] In combination with the XPS and FT-IR results, the adsorption performance of PBC was likely based on the cation exchange with the guest metal ions to generate the electrostatic bonds with the phosphate moieties on the BC surface (Fig. 15).[35,86–89] Therefore, the use of urea could provide more basic nitrogen sources to deprotonate the functionalized phosphate during the thermal treatment, thereby accelerating such ion exchange in the aqueous medium. Furthermore, the coordination of the remaining hydroxyl group in BC with the metal species could also contribute to the total metal uptake.[26,90]

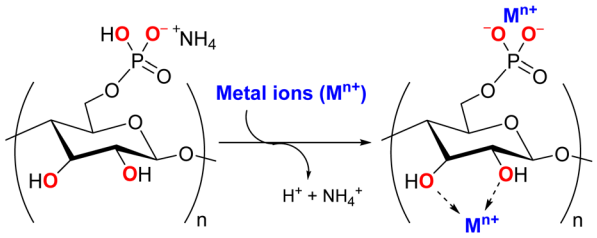

Fig. 15 Proposed adsorption mechanism.

Next, the influence of the initial metal ion concentration on the adsorption performance of modified cellulose was investigated (Fig. 16). A continuous and linear growth in the adsorption efficiency was obtained when the initial concentration of the metal ions increased from 0 to 350 ppm. Although higher

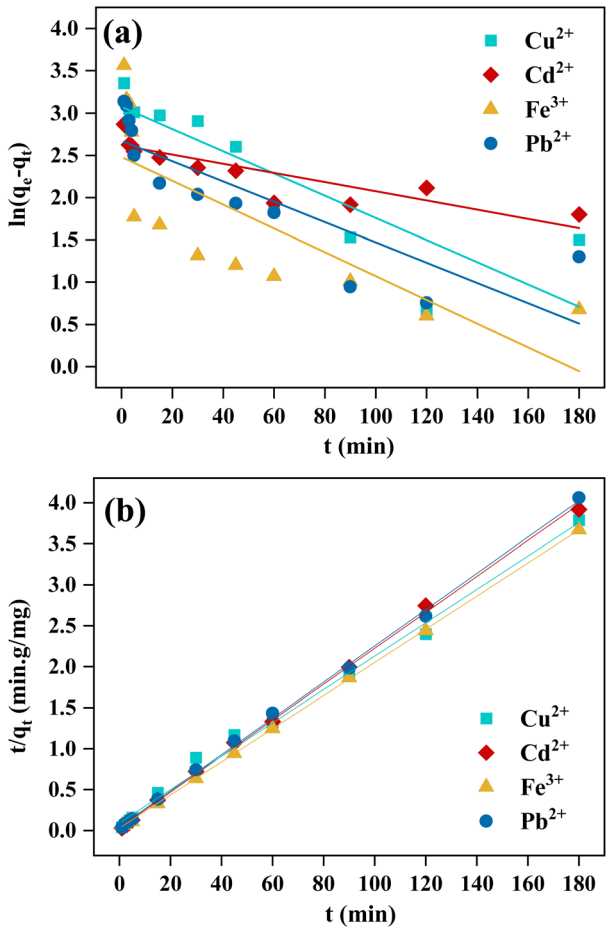

Fig. 14 Fitting of the time-dependent adsorption data with (a) the pseudo-first-order model and (b) the pseudo-second-order model.

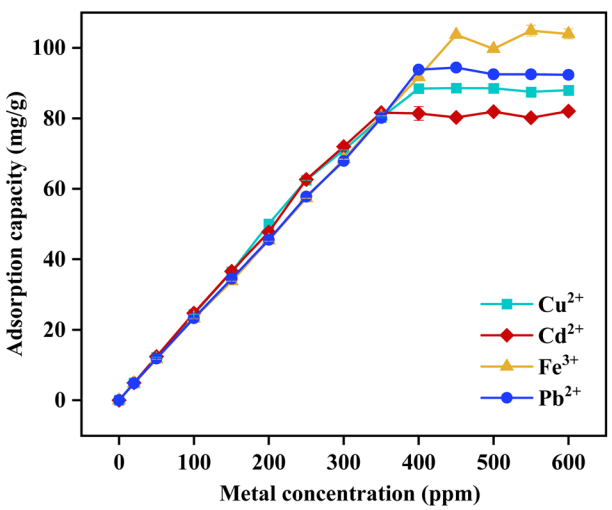

Fig. 16 Effect of the initial metal concentration on the adsorption capacity of PBC 150/1.0/9 (adsorption conditions: dosage 0.04 g/10 mL, temperature 30 °C, time 120 min, pH 5.0 ± 0.2, for Fe^{3+} pH 2.5).

initial concentrations are generally associated with a faster saturation of active sites due to increased competition among the metallic species,[91] the adsorption capacity of PBC continued to increase significantly for Cu^{2+}, Cd^{2+}, and Pd^{2+} ions, reaching maximum values in the range of approximately 80–90 mg g^{-1} at 400 ppm. At higher initial concentrations, no substantial changes in adsorption capacity were observed, indicating that 400 ppm represented the equilibrium concentration for most of the metal ions tested. The adsorption performance for Fe^{3+} was an exception, with a maximum adsorption capacity exceeding 100 mg g^{-1} at an initial metal concentration of 450 ppm. This was attributed to the outstanding positive charges of Fe^{3+} compared to other divalent cations, which interacted more efficiently with electron-rich phosphate groups.[85]

To gain more mechanistic insights into the isothermal adsorption process by PBC, the experimental adsorption data obtained at varied initial concentrations of the metal ions were fitted to the Langmuir and Freundlich models, with the corresponding isotherm plots presented in Fig. 17a and b and the related parameters presented in Table S2. The determination coefficients obtained from the Langmuir model were close to unity ($R^2 \geq 0.99$), in contrast to the Freundlich model, which yielded significantly lower correlation values ($R^2 \leq 0.86$), suggesting that monolayers of the tested metal ion species were adsorbed on the homogenous surface of PBC.[86] The theoretical maximum metal ion uptake (q_{max}), calculated using the Langmuir isotherm equation, served as a reference for evaluating and comparing the performance of various adsorbent materials. In this study, the maximum trapping capacities for Cu^{2+}, Cd^{2+}, Fe^{3+}, and Pb^{2+} were determined to be 120.03, 113.39, 168.39, and 141.75 mg g^{-1}, respectively. Notably, Fe^{3+} exhibited the highest adsorption capacity, likely due to its trivalent nature, different from the other divalent metal ions.

The solution pH value is considered as an essential factor in the aqueous adsorption, not only by controlling the charge on the adsorbent surface but also by influencing electrostatic interactions between the adsorbent and the adsorbate species.[92] The charge balance of a material in an electrolytic medium can be presented as the point of zero charge (PZC). In this study, the PZC of pure BC was determined to be 7.5, in good agreement with previously reported values for cellulose-based materials (Fig. S4).[37,93] Upon phosphorylation, the PZC of the sample PBC 150/1.0/9 decreased to 6.8, which closely aligns with values of phosphorylated cellulose synthesized using H_3PO_4 and $(NH_4)_2HPO_4$ reported in the literature (PZC ≈ 6.75).[94] This reduction in PZC indicated the successful incorporation of acidic functional groups, namely, phosphate-based moieties, on the bacterial cellulose surface. These groups, after deprotonation, could introduce more negative charges, lowering the overall surface potential. As a result, the modified bacterial cellulose network could exhibit stronger electrostatic attraction toward positively charged metal ions, enhancing its adsorption performance. The shift in PZC also indicated a significant change in the surface chemistry of the cellulose matrix, resulting from covalent phosphorylation. This modification not only increased the number of active sites but also enabled selective interactions with target species depending on the solution pH.

With increasing pH, the adsorption capacities for all tested metal ions gradually increased to above 80 mg g^{-1} (Fig. 18). This

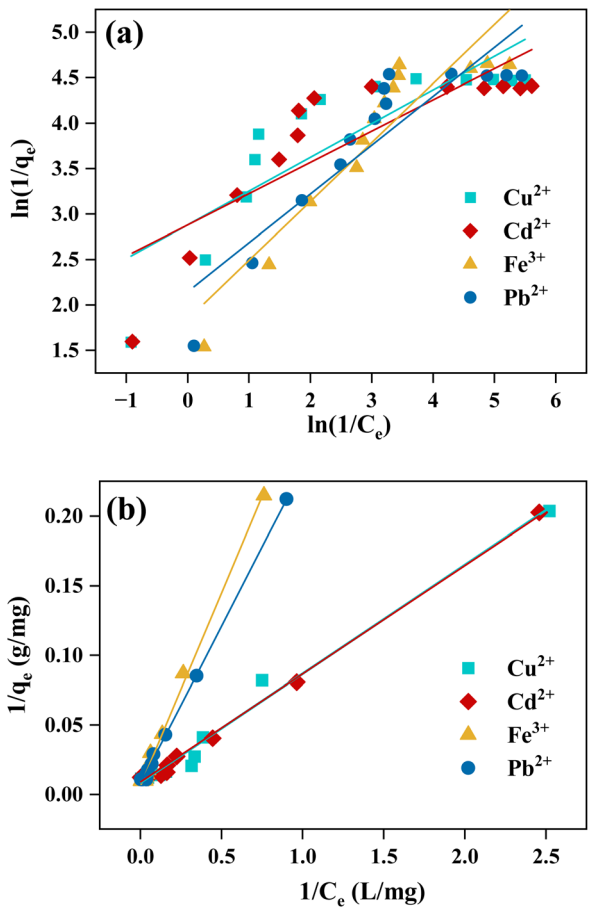

Fig. 17 Fitting the concentration-dependent adsorption results with (a) Freundlich isotherm adsorption model and (b) Langmuir isotherm adsorption model.

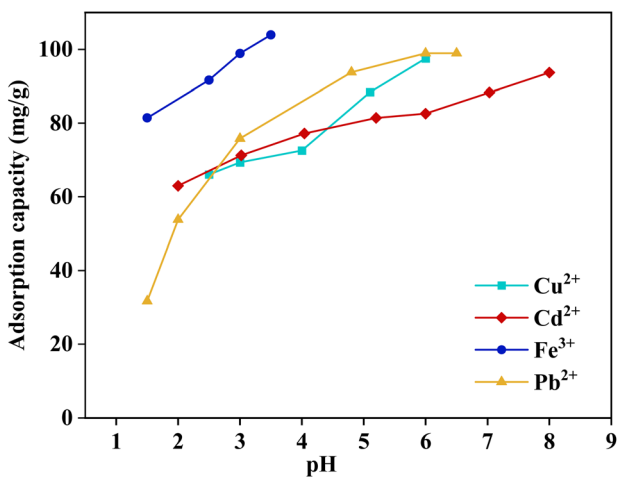

Fig. 18 Effect of the initial metal concentration on the adsorption capacity of PBC 150/1.0/9 (adsorption conditions: dosage 0.04 g/10 mL, concentration 400 ppm, temperature 30 °C, time 120 min).

enhancement was likely attributed to reduced electrostatic repulsion between the positively charged metal cations and the increasingly negative surface of the PBC. Therefore, the adsorbent exhibited a higher affinity for capturing metal ions at elevated pH levels.[37] In detail, the experiments for Cu^{2+} and Cd^{2+} revealed typical adsorption trends, with maximum capacities of 97.5 and 93.7 mg g^{-1}, respectively, at pH 6.0 and 3.5, suggesting a strong pH sensitivity for these ions. In contrast, Fe^{3+} presented a more gradual increase, affording the highest adsorption capacity among all tested ions—103.95 mg g^{-1} at pH 7.0. These results demonstrated that the solution pH value was a critical parameter in controlling the adsorption performance of cellulose-based materials for the metal ions. The pH-dependent adsorption performance could be driven by interaction between the surface functional groups and the guest ions, which thereby affects charge distribution and adsorption affinity.

In general, the adsorption capacities of PBC obtained for Cu^{2+}, Cd^{2+}, Fe^{3+}, and Pb^{2+} were comparable to or even significantly better than most previously reported values for cellulose-based adsorbents (Table 2). It should be noted that toxic and costly reagents and solvents were often required to fabricate these materials. For instance, cellulose paper was grafted with quinine in a multi-step procedure involving bromine, pyridine, *p*-toluenesulfonyl chloride, and many additives and organic solvents to enable trapping Cd^{2+} at a low capacity of 18.6 mg g^{-1} (entry 1).[95] Furthermore, relatively high metal uptakes (entries 6 and 9) were recorded for Cu^{2+}, Fe^{3+}, and Cd^{2+}, respectively, using cellulose phosphorylated with adenosine-5′-triphosphate and a composite phase of phosphorylated cellulose covered by electrospun chitosan-poly(ethylene oxide) nanofibers.[96,97] The combination of a 3D bacterial cellulose matrix and the $(NH_4)_2HPO_4$ salt allowed the incorporation of phosphate groups onto the cellulose chain under environmentally benign conditions, yielding significant results for the tested metal ions.

To highlight the efficiency of the phosphorylation, nine single cations, including Cu^{2+}, Ni^{2+}, Cr^{3+}, Cd^{2+}, Fe^{3+}, Zn^{2+}, Pb^{2+}, Co^{2+}, and Mn^{2+}, were used in the experiments involving either PBC or BC. These metals were chosen due to their widespread presence and known toxicity in natural and industrial wastewater systems. As shown in Fig. 19, significant enhancements (2.3–4.4 times) in the adsorption capacity of PBC were observed for these metal ions compared to unmodified BC, clearly demonstrating the critical role of surface functionalization in enhancing the metal-binding performance of cellulose-based adsorbents and the efficiency of the phosphorylation treatment. While the adsorption capacity of pure BC fluctuated within a poor range of 20.0 to 40.0 mg g^{-1}, PBC achieved

Table 2 Modified cellulose and phosphorylated cellulose adsorbents for the adsorption of heavy metal ions

Entry	Cellulose-based adsorbents	Functionalization reagent(s)	Adsorption conditions	q (mg g^{-1})	Ref.
1	Quinine-immobilized cellulose paper	Quinine-alkynes	25 °C, C_0 = 100 ppm, dose = 5 g L^{-1}	18.6 (Cd^{2+})	95
2	TEMPO oxidized cellulose nanofibrils	TEMPO, polyethyleneimine, NaBr, NaClO	30 °C, C_0 = 50 ppm, dose = 1 g L^{-1}	~45 (Cu^{2+})	98
3	Carboxymethylated cellulose fiber	Sodium chloroacetate	Room temperature, C_0 = 100 ppm, dose = 4.26 g L^{-1}	23.48 (Cu^{2+})	99
4	Amidoxime functionalized waste cigarette filters	Amidoxime	25 °C, C_0 = 500 ppm, dose = 4 g L^{-1}	25.65 (Cu^{2+}) 25.16 (Pb^{2+}) ~2.1 (Cd^{2+})	100
5	Thiol-functionalized cellulose nanofiber	3,3′-Dithiodipropionic acid	C_0 = 200 ppm, dose = 0.2 g L^{-1}	39.6 (Cu^{2+}) 30.0 (Cd^{2+}) 19.6 (Pb^{2+})	90
6	Phosphorylated cellulose derivatives	Adenosine-5′-triphosphate	Room temperature, C_0 = 62.5 ppm, dose = 2 g L^{-1}	117.0 (Cu^{2+}) 114.0 (Fe^{3+})	96
7	Phosphorylated nanocellulose paper	H_3PO_4	C_0 = 63.5 ppm, dose = 2.62 g L^{-1}	7.7–19.4 (Cu^{2+})	101
8	Phosphorylated cellulose microsphere	Urea, H_3PO_4, DMF	25 °C, C_0 = 100 ppm, dose = 10 g L^{-1}	108.5 (Pb^{2+})	102
9	Phosphorylated cellulose/chitosan-poly (ethylene oxide) nanofibers	Urea, phosphate ester	25 °C, C_0 = 100 ppm, dose = 0.5g L^{-1}	115.62 (Cd^{2+})	97
10	Hydrogel phase of phosphorylated unbleached kraft pulps	Urea, $(NH_4)_2HPO_4$	25 °C, C_0 = 50–400 ppm, dose = 2 g L^{-1}	~40 (Cu^{2+})	103
11	Lyophilized powder of phosphorylated bacterial cellulose	Urea, H_3PO_4, DMF	C_0 = 5.6, 6.4 ppm dose = 1.33 g L^{-1}	4.2 (Fe^{3+}) 4.8 (Cu^{2+})	30
12	Hydrogel phase of phosphorylated bacterial cellulose	Urea, $(NH_4)_2HPO_4$	30 °C, C_0 = 400 ppm, dose = 4 g L^{-1}	88.4 (Cu^{2+}) 81.4 (Cd^{2+}) 91.7 (Fe^{3+}) 93.8 (Pb^{2+})	This work

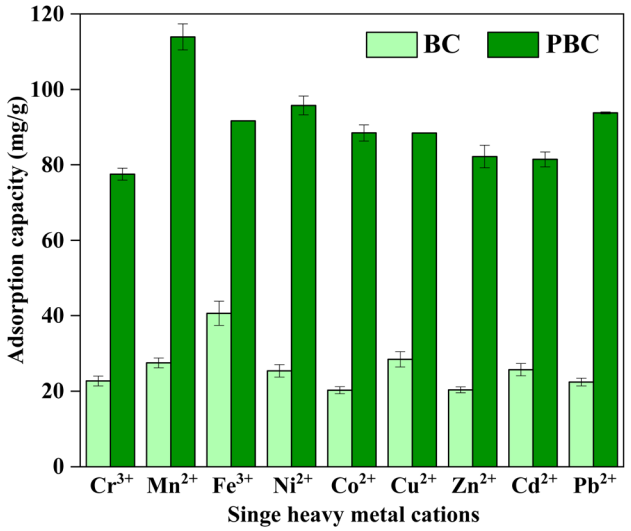

Fig. 19 Single-metal ion adsorption of BC and PBC 150/1.0/9 (adsorption conditions: dosage 0.04 g/10 mL, concentration 400 ppm, temperature 30 °C, time 120 min, pH 5.0 ± 0.2, for Fe^{3+} pH 2.5).

markedly higher capacities, ranging from 76.10 to 110.30 mg g^{-1}. The superior performance of PBC can be attributed to the presence of phosphate groups, which increase the number of electron-rich active sites on the cellulose surface, thereby promoting stronger electrostatic interactions and complexation with the positively charged metal ions. This functionalization not only improved adsorption capacity but also broadened the range of targetable metal species, making PBC a highly versatile and effective biomaterial for the removal of heavy metals from water. To elucidate the observed adsorption behaviour among different metal ions, various physicochemical factors such as ionic charge and ionic radius were considered. Several previous studies have suggested that ions with a higher charge and smaller radius, *e.g.*, Fe^{3+}, Cr^{3+}, tend to exhibit stronger adsorption due to their higher charge density, which facilitates stronger interactions with surface functional groups.[30,104] On the other hand, other reports argued that although a smaller ionic radius might promote the adsorption onto a heterogeneous surface, the resulting larger hydrated radius could lead to greater steric hindrance, thereby reducing accessibility to the adsorption sites.[105] Additionally, Pauling's electronegativity was proposed as another factor influencing the adsorption selectivity of varied metal ions.[105] Upon the results obtained in this study, without any consistent trend for the tested metal ions, it should be suggested that both mechanisms were important, and the adsorption of the metal ions was likely controlled by a complex combination of these factors rather than any single dominant parameter.

To expand the study to a complex wastewater medium, an aqueous solution containing nine metal ions, each at a concentration of 50 ppm, was prepared for the adsorption study. As previously reported, unmodified BC could capture all these ions, with capacities ranging from 5.12 to 7.74 mg g^{-1} (Fig. 20).[26] The phosphorylation allowed the adsorption of the

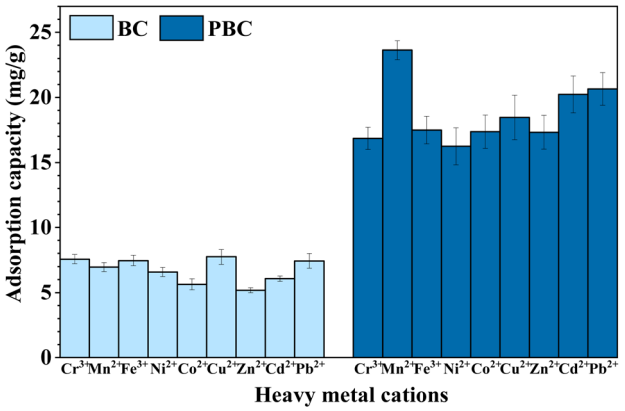

Fig. 20 Multi-metal ions adsorption of BC and PBC 150/1.0/9 (adsorption conditions: dosage 0.04 g/10 mL, concentration 50 ppm, temperature 30 °C, time 120 min, pH 3.0 ± 0.2).

multi-metal ions to significantly increase by 2.3–3.4 times, implying the great potential of PBC in the remediation of metal ions-containing wastewater. Like the single-metal ions test, the highest adsorption capacity of PBC was found for Mn^{2+} while the experiment using pure BC showed no clear differences in trapping the metal ions, indicating the superior selectivity of the modified functional groups with the Mn^{2+} species under competitive multi-metal conditions.

According to the proposed pseudo-second-order model, the adsorption of metal ions by PBC involved chemical interactions between the metal species and the functionalized sites on the cellulose backbone. This characteristic, therefore, enhanced the adsorption performance but caused significant challenges in the desorption of the metal ions, complicating the regeneration of PBC for the next use. Instead of inefficiently washing with water, the spent material was ion-exchanged with an NH_4Cl solution several times, allowing the removal of the adsorbed

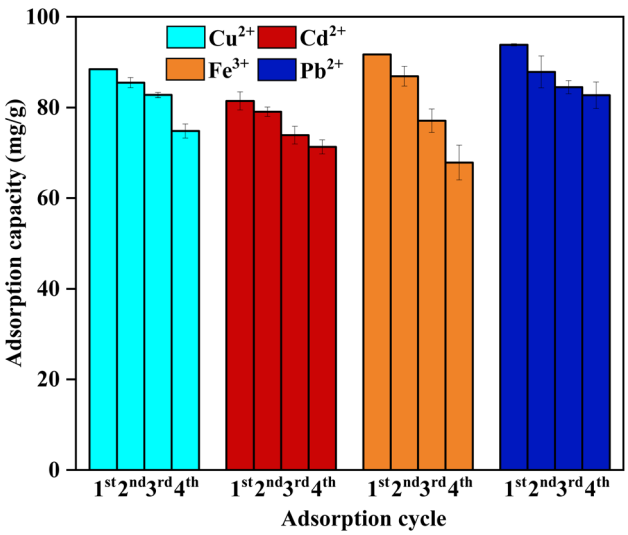

Fig. 21 Recycling tests for PBC 150/1.0/9 (adsorption conditions: dosage 0.04 g/10 mL, concentration 400 ppm, temperature 30 °C, time 120 min, pH 5.0 ± 0.2, for Fe^{3+} pH 2.5).

metal species from the PBC matrix. Alternatively, other chemicals such as HCl, $NaHCO_3$, and disodium ethylenediaminetetraacetate (Na_2EDTA) were previously required to recover phosphorylation-based adsorbents.[106,107] As expected, over four successive adsorption cycles, recycled PBC exhibited slight losses (12–16%) in the capture efficiency for Cu^{2+}, Cd^{2+}, and Pb^{2+}, while the adsorption of Fe^{3+} notably decreased by approximately 26% (Fig. 21). The strong affinity of Fe^{3+} species remaining at the adsorptive sites, which likely led to more Fe^{3+} species staying in the PBC matrix, preventing their exchange with the ammonium cation.

Conclusions

The present study introduced a straightforward and effective pathway to enrich the negative surface charge of bacterial cellulose through the successful incorporation of phosphate groups, enhancing the capacity to capture metal ions. Under appropriate conditions, the phosphorylated bacterial cellulose exhibited significantly improved adsorption capacities for a large number of the metal ions under both single- and multi-metal conditions. Kinetic and isotherm analyses further indicated that the adsorption process followed a pseudo-second-order kinetic model and was best described by the Langmuir isotherm. These findings supported chemisorption as the dominant mechanism, likely involving ion exchange and coordination between the metal ions and the functionalized cellulose surface. Furthermore, the adsorption capacities recorded in this study were comparable to the results reported for the cellulose-derived materials. The reusability of PBC was demonstrated over four single-metal adsorption cycles for Cu^{2+}, Cd^{2+}, Fe^{3+}, and Pb^{2+}, indicating PBC as a highly promising, biodegradable, and sustainable adsorbent for treating heavy metal-contaminated water. Its notable performance, combined with its low-cost production and tunable surface chemistry, can make it a viable alternative to conventional synthetic adsorbents. The demonstrated efficiency of PBC not only guides the functionalization approach to valorize bacterial cellulose but also facilitates the scaling up of bacterial cellulose-based materials in industrial and environmental applications. Our current study focuses on its reusability, regeneration efficiency, and development of flow systems for actual wastewater.

Author contributions

Conceptualization, H. V. L. and K. D. N.; data curation, D. D. B. N. and P. H. H.; methodology, P. H. H., K. D. N. and H. V. L.; analysis, U. T. N. V., A. T. H. P., L. H. T. N., and P. V. L.; writing – original draft, H. V. L. and D. D. B. N., writing – review and editing, P. H. H., and K. D. N., H. V. L., and P. V. L.; supervision, K. D. N., H. V. L, and P. H. H. All authors have read and agreed to the published version of the manuscript.

Conflicts of interest

The authors declare no competing financial interest.

Data availability

The authors indicate that the data supporting this article have been included as part of the supplementary information (SI). Supplementary information: overall XPS spectrum, FT-IR spectra, and calculated parameters of kinetic and isotherm models. See DOI: https://doi.org/10.1039/d5ra05752c.

Acknowledgements

This research is funded by Vietnam National University HoChiMinh City (VNU-HCM) under grant number: B2024-20-31. We acknowledge Ho Chi Minh City University of Technology (HCMUT), VNU-HCM for supporting this study.

References

1 A. G. Varghese, S. A. Paul and M. S. Latha, *Environ. Chem. Lett.*, 2019, **17**, 867–877.
2 N. A. A. Qasem, R. H. Mohammed and D. U. Lawal, *npj Clean Water*, 2021, **4**, 36.
3 J. Kushwaha and R. Singh, *Inorg. Chem. Commun.*, 2023, **152**, 110721.
4 B. Pratap, S. Kumar, S. Nand, I. Azad, R. N. Bharagava, L. F. Romanholo Ferreira and V. Dutta, *Chemosphere*, 2023, **313**, 137547.
5 M. Sabelfeld, L. Streckwall, B. Xuan-Thanh and S.-U. Geißen, *Case Stud. Chem. Environ. Eng.*, 2022, **5**, 100169.
6 A. Jan, M. Azam, K. Siddiqui, A. Ali, I. Choi and Q. Haq, *Int. J. Mol. Sci.*, 2015, **16**, 29592–29630.
7 M. Taseidifar, F. Makavipour, R. M. Pashley and A. F. M. M. Rahman, *Environ. Technol. Innovation*, 2017, **8**, 182–190.
8 X. Pei, L. Gan, Z. Tong, H. Gao, S. Meng, W. Zhang, P. Wang and Y. Chen, *J. Hazard. Mater.*, 2021, **406**, 124746.
9 R. K. Gautam, S. K. Sharma, S. Mahiya and M. C. Chattopadhyaya, in *Heavy Metals in Water*, Royal Society of Chemistry, Cambridge, 2014, pp. 1–24, DOI: 10.1039/9781782620174-00001.
10 S. Satyro, M. Race, R. Marotta, M. Dezotti, D. Spasiano, G. Mancini and M. Fabbricino, *J. Environ. Chem. Eng.*, 2014, **2**, 1969–1979.
11 M. Takht Ravanchi, T. Kaghazchi and A. Kargari, *Desalination*, 2009, **235**, 199–244.
12 G. McMullan, C. Meehan, A. Conneely, N. Kirby, T. Robinson, P. Nigam, I. M. Banat, R. Marchant and W. F. Smyth, *Appl. Microbiol. Biotechnol.*, 2001, **56**, 81–87.
13 M. M. Matlock, B. S. Howerton and D. A. Atwood, *Water Res.*, 2002, **36**, 4757–4764.
14 S. Zhang, Q. Shi, C. Christodoulatos, G. Korfiatis and X. Meng, *Chem. Eng. J.*, 2019, **370**, 1262–1273.
15 X. Yang, Y. Wan, Y. Zheng, F. He, Z. Yu, J. Huang, H. Wang, Y. S. Ok, Y. Jiang and B. Gao, *Chem. Eng. J.*, 2019, **366**, 608–621.
16 M.-Y. Chang and R.-S. Juang, *J. Colloid Interface Sci.*, 2004, **278**, 18–25.

17 D. B. Menezes, F. M. Diz, L. F. Romanholo Ferreira, Y. Corrales, J. R. V. Baudrit, L. P. Costa and M. L. Hernández-Macedo, *Cellulose*, 2021, **28**, 4137–4149.
18 A. Jamshaid, A. Hamid, N. Muhammad, A. Naseer, M. Ghauri, J. Iqbal, S. Rafiq and N. S. Shah, *ChemBioEng Rev.*, 2017, **4**, 240–256.
19 A. M. Elgarahy, K. Z. Elwakeel, S. H. Mohammad and G. A. Elshoubaky, *Clean Eng. Technol.*, 2021, **4**, 100209.
20 M. G. L. Ramírez, K. G. Satyanarayana, S. Iwakiri, G. B. de Muniz, V. Tanobe and T. S. Flores-Sahagun, *Carbohydr. Polym.*, 2011, **86**, 1712–1722.
21 S. Yang, S. Fu, H. Liu, Y. Zhou and X. Li, *J. Appl. Polym. Sci.*, 2011, **119**, 1204–1210.
22 Z. Cheng, R. Yang, X. Liu, X. Liu and H. Chen, *Bioresour. Technol.*, 2017, **234**, 8–14.
23 A. Ait Benhamou, Z. Kassab, M. Nadifiyine, M. H. Salim, H. Sehaqui, A. Moubarik and M. El Achaby, *Cellulose*, 2021, **28**, 4625–4642.
24 H. T. Phan, K. D. Nguyen, H. H. M. Nguyen, N. T. Dao, P. T. K. Le and H. V. Le, *Bioresour. Technol. Rep.*, 2023, **24**, 101613.
25 F. G. Blanco Parte, S. P. Santoso, C.-C. Chou, V. Verma, H.-T. Wang, S. Ismadji and K.-C. Cheng, *Crit. Rev. Biotechnol.*, 2020, **40**, 397–414.
26 H. M. H. Nguyen, C. D. Pham, K. D. Nguyen, A. T. T. Tran, N. T. H. Le, P. H. Ho and H. V. Le, *Chem. Eng. Technol.*, 2023, **46**, 2547–2559.
27 T. Sun, H. Wang, J. Liu, X. Chu, X. Xing, S. Liu, E. Tang, X. Liu and D. Hildebrandt, *Cellulose*, 2021, **28**, 4151–4164.
28 M. K. Patoary, A. Farooq, B. Zaarour and L. Liu, *Cellulose*, 2021, **28**, 4105–4117.
29 M. Hadid, H. Noukrati, H. Ben youcef, A. Barroug and H. Sehaqui, *Cellulose*, 2021, **28**, 7893–7908.
30 T. Oshima, K. Kondo, K. Ohto, K. Inoue and Y. Baba, *React. Funct. Polym.*, 2008, **68**, 376–383.
31 T. Oshima, S. Taguchi, K. Ohe and Y. Baba, *Carbohydr. Polym.*, 2011, **83**, 953–958.
32 N. Boonchai, W. Mongkolthanaruk, V. Harnchana, K. Faungnawakij and S. Pinitsoontorn, *Biointerface Res. Appl. Chem.*, 2021, **12**, 1587–1600.
33 M. S. Alhumaimess, I. H. Alsohaimi, A. A. Alqadami, M. M. Kamel, M. Naushad, T. Ahamad and H. Alshammari, *J. Sol-Gel Sci. Technol.*, 2019, **89**, 602–615.
34 G. Hou, S. Zhao, L. Peng, Z. Fang and A. Isogai, *Cellulose*, 2022, **29**, 7365–7376.
35 E.-H. Ablouh, Z. Kassab, F.-z. Semlali Aouragh Hassani, M. El Achaby and H. Sehaqui, *RSC Adv.*, 2022, **12**, 1084–1094.
36 S. Kongruang, *Appl. Biochem. Biotechnol.*, 2008, **148**, 245–256.
37 H. V. Le, N. T. Dao, H. T. Bui, P. T. Kim Le, K. A. Le, A. T. Tuong Tran, K. D. Nguyen, H. H. Mai Nguyen and P. H. Ho, *ACS Omega*, 2023, **8**, 33412–33425.
38 T. Petreus, B. A. Stoica, O. Petreus, A. Goriuc, C.-E. Cotrutz, I.-V. Antoniac and L. Barbu-Tudoran, *J. Mater. Sci.: Mater. Med.*, 2014, **25**, 1115–1127.
39 M. H. Kudzin, Z. Mrozińska and P. Urbaniak, *Antibiotics*, 2021, **10**, 1–27.
40 R. D. S. Bezerra, A. I. S. Morais, J. A. Osajima, L. C. C. Nunes and E. C. Silva Filho, *Int. J. Biol. Macromol.*, 2016, **86**, 362–375.
41 J. N. Putro, S. P. Santoso, S. Ismadji and Y.-H. Ju, *Microporous Mesoporous Mater.*, 2017, **246**, 166–177.
42 M. Kröger, O. Badara, T. Pääkkönen, I. Schlapp-Hackl, S. Hietala and E. Kontturi, *Biomacromolecules*, 2023, **24**, 1318–1328.
43 A. Anand, B. Unnikrishnan, C. Y. Wang, J. Y. Lai, H. J. Lin and C. C. Huang, *npj Clean Water*, 2024, **7**, 84.
44 C. Jiao, Z. Zhang, J. Tao, D. Zhang, Y. Chen and H. Lin, *RSC Adv.*, 2017, **7**, 27787–27795.
45 S. Pal, R. Nisi, M. Stoppa and A. Licciulli, *ACS Omega*, 2017, **2**, 3632–3639.
46 M. A. Signore, S. K. Padmanabhan, L. Velardi, A. Serra, M. Stoppa, L. Francioso and A. Licciulli, *Appl. Surf. Sci.*, 2025, **692**, 162734.
47 S. K. Padmanabhan, F. Lionetto, R. Nisi, M. Stoppa and A. Licciulli, *Sustainability*, 2022, **14**, 2247.
48 J. Gao, L. Qu, J. Qian, Z. Wang, Y. Li, S. Yi and Z. He, *Sci. Rep.*, 2020, **10**, 6760.
49 J. Wu, Z. Yixiu, T. Zhong, W. Zhang and H. Chen, *J. Wood Sci.*, 2023, **69**, 13.
50 M.-C. Popescu, C.-M. Popescu, G. Lisa and Y. Sakata, *J. Mol. Struct.*, 2011, **988**, 65–72.
51 M. M. Gomaa, C. Hugenschmidt, M. Dickmann, E. E. Abdel-Hady, H. F. M. Mohamed and M. O. Abdel-Hamed, *Phys. Chem. Chem. Phys.*, 2018, **20**, 28287–28299.
52 N. F. Vasconcelos, J. P. A. Feitosa, F. M. P. da Gama, J. P. S. Morais, F. K. Andrade, M. d. S. M. de Souza Filho and M. d. F. Rosa, *Carbohydr. Polym.*, 2017, **155**, 425–431.
53 T. Chu, Z. Zhou, P. Tian, T. Yu, C. Lian, B. Zhang and F.-Z. Xuan, *Nat. Commun.*, 2024, **15**, 7329.
54 V. Hospodarova, E. Singovszka and N. Stevulova, *Am. J. Anal. Chem.*, 2018, **09**, 303–310.
55 M. El Achaby, Z. Kassab, A. Barakat and A. Aboulkas, *Ind. Crops Prod.*, 2018, **112**, 499–510.
56 M. Poletto, H. Ornaghi and A. Zattera, *Materials*, 2014, **7**, 6105–6119.
57 E.-H. Ablouh, F. Brouillette, M. Taourirte, H. Sehaqui, M. El Achaby and A. Belfkira, *RSC Adv.*, 2021, **11**, 24206–24216.
58 W. D. Wanrosli, R. Rohaizu and A. Ghazali, *Carbohydr. Polym.*, 2011, **84**, 262–267.
59 R. J. Coleman, G. Lawrie, L. K. Lambert, M. Whittaker, K. S. Jack and L. Grøndahl, *Biomacromolecules*, 2011, **12**, 889–897.
60 S. Wu, Y. Gong, S. Liu, Y. Pei and X. Luo, *Carbohydr. Polym.*, 2021, **254**, 117421.
61 J.-F. Zhang and R.-C. Tang, *Cellulose*, 2023, **30**, 10733–10748.
62 N. D. Shooto, *Surf. Interfaces*, 2020, **20**, 100624.
63 A. Rahman, K. Yoshida, M. M. Islam and G. Kobayashi, *Sustainability*, 2023, **15**, 4470.
64 V. Kokol, M. Božič, R. Vogrinčič and A. P. Mathew, *Carbohydr. Polym.*, 2015, **125**, 301–313.

65 L. C. Yeng, M. U. Wahit and N. Othman, *J. Teknol. Lab.*, 2015, **75**, 107–112.
66 D. Aoki and Y. Nishio, *Cellulose*, 2010, **17**, 963–976.
67 G. Nourry, D. Belosinschi, M. P. Boutin, F. Brouillette and R. Zerrouki, *Cellulose*, 2016, **23**, 3511–3520.
68 M. Šetka, R. Calavia, L. Vojkůvka, E. Llobet, J. Drbohlavová and S. Vallejos, *Sci. Rep.*, 2019, **9**, 8465.
69 R. Dalmis, S. Köktaş, Y. Seki and A. Ç. Kılınç, *Cellulose*, 2020, **27**, 127–139.
70 Y. Wen, J. Ding, Y. Yang, X. Lan, J. Liu, R. Hu and M. Zhu, *Adv. Funct. Mater.*, 2022, **32**, 2109377.
71 J. Gong, J. Li, J. Xu, Z. Xiang and L. Mo, *RSC Adv.*, 2017, **7**, 33486–33493.
72 W. Wang, Y. Kan, H. Pan, Y. Pan, B. Li, K. M. Liew and Y. Hu, *Composites, Part A*, 2017, **94**, 170–177.
73 J. S. Stevens, S. Coultas, C. Jaye, D. A. Fischer and S. L. M. Schroeder, *Phys. Chem. Chem. Phys.*, 2020, **22**, 4916–4923.
74 Y. Wu, Q. Fang, X. Yi, G. Liu and R. W. Li, *Prog. Nat. Sci.:Mater. Int.*, 2017, **27**, 514–519.
75 M. Ghanadpour, F. Carosio, P. T. Larsson and L. Wågberg, *Biomacromolecules*, 2015, **16**, 3399–3410.
76 L. Bahsis, E.-H. Ablouh, Z. Hanani, H. Sehaqui, M. El Achaby, M. Julve and S.-E. Stiriba, *Carbohydr. Polym.*, 2024, **324**, 121501.
77 H. Huo, Y. Yu, X. Zhang, M. Tang, C. Chen, S. Wang and D. Min, *Ind. Crops Prod.*, 2022, **188**, 115727.
78 L. Passauer and H. Bender, *Carbohydr. Polym.*, 2017, **168**, 356–364.
79 M. Zhao, Y. Ono, Y. Noguchi, S. Fujisawa and T. Saito, *Cellulose*, 2022, **29**, 2805–2816.
80 M. Tavakoli, B. Mazela, W. Grześkowiak, J. Proch, M. Mleczek and W. Perdoch, *Molecules*, 2023, **29**, 133.
81 S. Boukind, J. Bouaouina, H. Bouras, A. A. Benhamou, E. H. Ablouh, Z. Kassab, M. Khouloud, M. El Achaby and H. Sehaqui, *Int. J. Biol. Macromol.*, 2022, **219**, 949–963.
82 F. Rol, C. Sillard, M. Bardet, J. R. Yarava, L. Emsley, C. Gablin, D. Léonard, N. Belgacem and J. Bras, *Carbohydr. Polym.*, 2020, **229**, 115294.
83 D. Robati, *J. Nanostruct. Chem.*, 2013, **3**, 55.
84 S. M. Al-Jubouri, S. I. Al-Batty, R. Ramsden, J. Tay and S. M. Holmes, *Desalin. Water Treat.*, 2021, **236**, 171–181.
85 E. Mahmoudi, S. Azizkhani, A. W. Mohammad, L. Y. Ng, A. Benamor, W. L. Ang and M. Ba-Abbad, *J. Environ. Sci.*, 2020, **98**, 151–160.
86 H. A. Said, I. Ait Bourhim, A. Ouarga, I. Iraola-Arregui, M. Lahcini, A. Barroug, H. Noukrati and H. Ben youcef, *Int. J. Biol. Macromol.*, 2023, **225**, 1107–1118.
87 L. V. A. Gurgel, J. C. Perin de Melo, J. C. de Lena and L. F. Gil, *Bioresour. Technol.*, 2009, **100**, 3214–3220.
88 N. Zhang, J. Li, B. Tian, J. Zhang, T. Li, Z. Li, Y. Wang, Z. Liu, H. Zhao and F. Ma, *J. Radioanal. Nucl. Chem.*, 2023, **332**, 173–183.
89 M. G. Tokmachev, N. A. Tikhonov and R. K. Khamizov, *React. Funct. Polym.*, 2008, **68**, 1245–1252.
90 H. Y. Choi, J. H. Bae, Y. Hasegawa, S. An, I. S. Kim, H. Lee and M. Kim, *Carbohydr. Polym.*, 2020, **234**, 115881.
91 L. Zheng, D. Peng, S. Zhang, Y. Yang, L. Zhang and P. Meng, *Environ. Sci. Pollut. Res.*, 2020, **27**, 43246–43261.
92 I. Elsayed, G. T. Schueneman, E. M. El-Giar and E. B. Hassan, *Gels*, 2023, **9**, 154.
93 Y. Kemal Recepoglu and A. YÜKsel, *Cellul. Chem. Technol.*, 2021, **55**, 385–401.
94 M. A. Abdel Khalek, I. Osama, I. O. Abdelwahed, K. A. Selim, F. I. El Hosiny, M. A. Abdel Khalek, I. Osama and I. Osama Kinetics, *Colloid and Surface Science*, 2017, **2**, 47–53.
95 E. C. Aka, M. C. Nongbe, T. Ekou, L. Ekou, V. Coeffard and F.-X. Felpin, *J. Environ. Sci.*, 2019, **84**, 174–183.
96 P. Liu, P. F. Borrell, M. Božič, V. Kokol, K. Oksman and A. P. Mathew, *J. Hazard. Mater.*, 2015, **294**, 177–185.
97 R. Brandes, F. Brouillette and B. Chabot, *J. Appl. Polym. Sci.*, 2021, **138**, 50021.
98 N. Zhang, G.-L. Zang, C. Shi, H.-Q. Yu and G.-P. Sheng, *J. Hazard. Mater.*, 2016, **316**, 11–18.
99 J. Wang, M. Liu, C. Duan, J. Sun and Y. Xu, *Carbohydr. Polym.*, 2019, **206**, 837–843.
100 Y. Yue, Y. Liu, W. Zhang, J. Guo, Y. Gong and Y. Yu, *J. Environ. Chem. Eng.*, 2022, **10**, 107846.
101 A. Mautner, H. Maples, T. Kobkeatthawin, V. Kokol, Z. Karim, K. Li and A. Bismarck, *Int. J. Environ. Sci. Technol.*, 2016, **13**, 1861–1872.
102 X. Luo, J. Yuan, Y. Liu, C. Liu, X. Zhu, X. Dai, Z. Ma and F. Wang, *ACS Sustain. Chem. Eng.*, 2017, **5**, 5108–5117.
103 I. Carrillo-Varela, M. Albornoz, I. Reyes-Gonzalez, M. G. Aguayo, E. Elgueta, P. Reyes-Contreras, M. Pereira and R. T. Mendonça, *Cellulose*, 2024, **31**, 7629–7660.
104 T. Bohli, A. Ouederni and I. Villaescusa, *Euro-Mediterranean Journal for Environmental Integration*, 2017, 2.
105 M. Arshadi, M. J. Amiri and S. Mousavi, *Water Resour. Ind.*, 2014, **6**, 1–17.
106 N. Zhang, W. Li, J. Li, Q. Wang, B. Li, J. Zhang, T. Zhang, Z. Li, Y. Li, B. Tian and H. Zhao, *Sep. Purif. Technol.*, 2025, **368**, 132907.
107 N. Srivastava, A. K. Thakur and V. K. Shahi, *Carbohydr. Polym.*, 2016, **136**, 1315–1322.